

# Image Segmentation Based on Multi-region Multi-scale Local Binary Fitting and Kullback-Leibler Divergence

Dansong Cheng, Feng Tian, Lin Liu, Xiaofang Liu and Ye Jin

**Abstract**—The inhomogeneity of intensity and the noise of image are the two major obstacles to accurate image segmentation by region-based level set models. To provide a more general solution to these challenges and address the difficulty of image segmentation methods to handle an arbitrary number of regions, we propose a region-based multi-phase level set method, which is based on the multi-scale local binary fitting (MLBF) and the Kullback-Leibler (KL) divergence, called KL-MMLBF. We first apply the multi-scale theory and multi-phase level set framework to the local binary fitting model to build the multi-region multi-scale local binary fitting (MMLBF). Then the energy term measured by KL divergence between regions to be segmented is incorporated into the energy function of MMLBF. KL-MMLBF utilizes the between-cluster distance and the adaptive kernel function selection strategy to formulate the energy function. Being more robust to the initial location of the contour than the classical segmentation models, KL-MMLBF can deal with blurry boundaries and noise problems. The results of experiments on synthetic and medical images have shown that KL-MMLBF can improve the effectiveness of segmentation while ensuring the accuracy by accelerating this minimization of this energy function and the model has achieved better segmentation results in terms of both accuracy and efficiency to analyze the multi-region image.

**Index Terms**—Image segmentation, Kullback-Leibler divergence, Multi-scale Local Binary Fitting, Multi-region, Active contour model

## I. INTRODUCTION

**I**MAGE segmentation is a process of partitioning an image into homogeneous regions according to the image's features such as color, texture, shape, etc. [1], and it is very important for visual information analysis processes such as object detection [2], computer vision [3]. A number of segmentation algorithms have been proposed over the last few decades [4], [5], [6], [7], [8], [9], [10], [11], [12], [13], [14], [15]. Amongst the approaches, the active contour model (ACM) proposed by Kass et al. [6] is one of the most successful PDE-based models. However, ACM has some drawbacks such as its difficulty in handling topological changes and its dependency on parameterization.

To overcome the drawbacks, many methods have been proposed. The Chan-Vese (CV) model [9] has advantages in

processing images with weak boundaries and is able to detect an object's inside contour. However, since CV assumes that regions to segment are intensity homogeneous, it cannot be directly applied to the inhomogeneous intensity image represented by the means of piecewise constants. Based on the level set model [10], the Local Binary Fitting (LBF) model [12], Local Chan-Vese (LCV) model [16], Local and Global Intensity Fitting (LGIF) model [17] were proposed during last decades to improve the segmentation ability of CV model. As a result both the segmentation efficiency and effectiveness of these models are enhanced. But these models are sensitive to the position of the initial curve and come with the higher computational complexity. Liu and Cheng [18] propose a novel region-based model (KL-MLBF model), which adopts multi-scale theory into LBF model and modifies the energy function by incorporating a new energy term (Kullback-Leibler divergence [19]) expressed as between-cluster distance. By maximizing the new term, KL-MLBF achieves segmentation of high accuracy term.

Despite of the advantages above, one main problem of the level set representation lies in the fact that a level set function is restricted to the separation of two regions. To alleviate this limitation of the level set, many methods have adapted the level set for multiple region segmentation such as MRI of the abdomen, aerial images of crops and farmlands, images and videos of sporting events [10], [20], [21], [22], [23]. Most of these approaches use  $N$  level set functions to segment  $N$  objects and rely on coupling terms to avoid overlaps and gaps [21], [24]. These methods have the advantage that each object can be independently specified in both its own topology and its internal and external speeds. However, coupling terms do not forbid certain object interactions, so these approaches can still produce overlaps and gaps in practice. As well, most are not formulated to consider the relationships between objects, and memory requirements become daunting as the number of objects to be segmented grows. In [25], a level set function is assigned to each region. This framework has been adapted to classification in [26]. In another approach, the bi-model case is extended to tri-model segmentation [27]. Both techniques, however, assume an initially fixed number of regions. This assumption is omitted in [21] where the number of regions is estimated in a preliminary stage by means of a Gaussian mixture estimate of the image histogram. This way, the number of mixture coefficients determines the number of regions. However, this kind of estimation is only loosely connected to the energy functional that is minimised. A considerably

The authors D Cheng, L Liu and Y Jin are with the School of Computer Science and Technology, Harbin Institute of Technology, 92 West Dazhi Street, Nan Gang District, Harbin, 150001, P.R.China.

The author X Liu is with the School of Electrical Engineering and Automation, Harbin Institute of Technology, P.R.China.

The author F Tian is with the Faculty of Science & Technology, Bournemouth University, UK.

Xiaofang Liu, e-mail: liuxf@hit.edu.cn.

different approach is proposed in [8], where the level set functions are used in such a way that  $N$  regions are represented by only  $\log_2 N$  level set functions. Unfortunately, this will result in empty regions if less than  $N$  regions are present in the image. These empty regions have undefined statistics, though the statistics still appear in the evolution equations. Leventon et al. [28] use a Gaussian model to describe their shape priors. They assume a uniform distribution over pose parameters that include translation and rotation. Paragios and Deriche [21] avoid this assumption by calculating the means of a Gaussian mixture estimation of the image histogram. The number of mixture coefficients determines the number of regions to be segmented. Altogether, the prominence of level set based segmentation is yet lost as soon as more than two regions come into play.

In this paper, we extend the KL-MLBF model and generalize multi-phase level set framework which can handle the multi-region inhomogeneous images segmentation. We call our new model as KL-MMLBF.

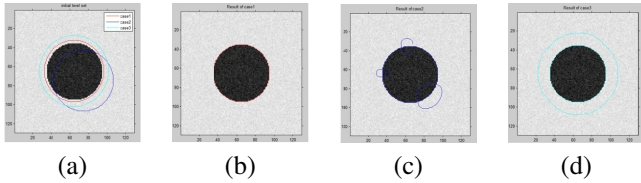


Fig. 1. The sensitivity to initial location of level set function in LBF (a) Three kinds of initialization of the level set function; (b)-(d) The segmentation results of the corresponding LBF model

## II. KULLBACK-LEIBLER DIVERGENCE INCORPORATED WITH MULTI-REGION MULTI-SCALE LOCAL BINARY FITTING

The sensitivity of the local binary fitting model to the initial position of the level set is illustrated in Fig.1. Although the variation of the initialization position is very small, as shown in Fig.1 (a), the segmentation results are quite different, as shown in Fig.1 (b)-(d). Obviously, the model is very sensitive to the initial position. The analysis of the force generated by the model shows that, for binary image, the force is "borderline", i.e. the larger the contrast in the region is, the stronger the force in the models. Likewise, the smaller the image contrast is, the weaker the force of the model is. So when the initialization level set is away from the boundary of the target, the level set evolves slowly. As the zero level set approaches the border region, it will evolve more quickly. A new zero level set will derive soon, and it's easy to cause "double ring" effect, as shown in Fig.1 (d). Consequently, the model can only achieve local solution. The main cause of the local force is the Gauss kernel used in LBF model. Comparing the LBF model and the Chan-Vese model, we can conclude that: (1) the kernel size of LBF model in the level set is inversely related to the initial position and the sensitive to Gauss noise; (2) The kernel size of LBF model is proportional to processing precision of the segmentation of inhomogeneous image.

To overcome the sensitivity to initial position and enhance the robustness to noise of the level set of existing models, we

present in this section our proposed KL-MMLBF model which is based on KL divergence and multi-region multi-scale local binary fitting (MMLBF). The KL-MMLBF model, which can be regarded as an extended or improved LBF model, is more robust to the initial position of the level set and Gaussian noise. It can also reduce the number of iterations required for convergence. Compared with other classical segmentation models such as LBF, LGIF and LCV, KL-MMLBF is more effective to deal with the non-uniform image segmentation and multi-region image.

### A. Multi-region Multi-scale Local Binary Fitting Model (MMLBF)

In order to solve multi-region image segmentation problem, we extend the MLBF model to multi-region, as shown in Fig. 2, where  $m$  is the level set number. The two level set functions split the image into three non-overlapping sub regions in Fig. 2(a), and in Fig. 2(b) the two level set functions split the image into four non-overlapping sub regions. We use the energy functional extremum problem shown in Eq.(1) to describe the multi-region multi-scale local binary fitting model (MMLBF):

$$E^{MMLBF} = \sum_{j=1}^n w_j E_{\mathbf{x}}^{\sigma_j}(f_{1,j}(\mathbf{x}), f_{N,j}(\mathbf{x})) \quad (1)$$

where

$$E_{\mathbf{x}}^{\sigma_j}(f_{1,j}(\mathbf{x}), f_{N,j}(\mathbf{x})) = \sum_{i=1}^N \lambda_i \int_{\Omega_i} K_{\sigma_j}(\mathbf{x}-\mathbf{y}) |I(\mathbf{y}) - f_{i,j}(\mathbf{x})|^2 d\mathbf{y}$$

$$K_{\sigma_j}(x-y) = \frac{1}{(2\pi)^{1/2} \sigma_j} \exp^{-\frac{|x-y|^2}{2\sigma_j^2}}$$

where  $N = 2^m$  is number of partition areas. The definition of other parameters is the same as that in the MLBF model [18].

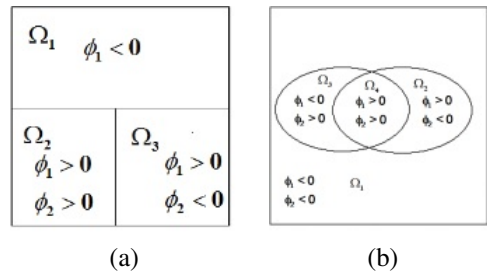


Fig. 2. Illustration of multi region image segmentation. (a) Domain partition into 3 regions, (b) Domain partition into 4 regions

### B. Formulation of the Level Set Model

To illustrate the formulation, we start with the multi-region multi-scale level set to solve the minimization of the energy function. Take 4-phase image segmentation model as an example, for the purpose of illustration, let us write the above energy for  $N = 2^m = 4$  phases or classes (and therefore using  $m=2$  level set functions). The two-step iterative method steps are as follows.

Firstly, fix the level set function, update  $\phi_k(x)$ ,  $k = 1, 2$ ; updates  $f_{i,j}$ ,  $i = 1, 2, 3, 4$ ,  $j = 1, \dots, n$ , according to Eq. (2).

$$\begin{aligned} \varepsilon(\phi) &= \sum_{i=1}^4 \gamma_2 \int P(I(\mathbf{x}))_{\Omega_i} \log \frac{P(I(\mathbf{x}))_{\Omega_i}}{P(I(\mathbf{x}))_{\Omega_i \setminus C_i}} d\mathbf{x} \\ &+ \sum_{j=1}^n w_j \sum_{i=1}^4 \lambda_i \int_{\Omega_i} K_{\sigma_j}(\mathbf{y} - \mathbf{x}) |I(\mathbf{x}) - f_{i,j}(\mathbf{y})|^2 M_i(\phi(\mathbf{x})) d\mathbf{x} \\ &+ v \int |\nabla H(\phi(\mathbf{x}))| d\mathbf{x} + \mu \int \frac{1}{2} (|\nabla \phi(\mathbf{x})| - 1)^2 d\mathbf{x} \end{aligned} \quad (2)$$

where

$$\begin{cases} f_{i,j}(\mathbf{y}) = \frac{K_{\sigma_j}(\mathbf{y}-\mathbf{x}) * (M_i^\varepsilon(\phi_1(\mathbf{x}), \phi_2(\mathbf{x})) I(\mathbf{x}))}{K_{\sigma_j}(\mathbf{y}-\mathbf{x}) * N_i^\varepsilon(\phi_1(\mathbf{x}), \phi_2(\mathbf{x}))} \\ M_1^\varepsilon(\phi_1(\mathbf{x}), \phi_2(\mathbf{x})) = H_\varepsilon(\phi_1(\mathbf{x})) \cdot H_\varepsilon(\phi_2(\mathbf{x})), \\ M_2^\varepsilon(\phi_1(\mathbf{x}), \phi_2(\mathbf{x})) = (1 - H_\varepsilon(\phi_1(\mathbf{x}))) \cdot H_\varepsilon(\phi_2(\mathbf{x})), \\ M_3^\varepsilon(\phi_1(\mathbf{x}), \phi_2(\mathbf{x})) = H_\varepsilon(\phi_1(\mathbf{x})) \cdot (1 - H_\varepsilon(\phi_2(\mathbf{x}))), \\ M_4^\varepsilon(\phi_1(\mathbf{x}), \phi_2(\mathbf{x})) = (1 - H_\varepsilon(\phi_1(\mathbf{x}))) \cdot (1 - H_\varepsilon(\phi_2(\mathbf{x}))) \end{cases}$$

$\int |\nabla H(\phi(\mathbf{x}))| d\mathbf{x}$  is the regularization term for the length of the zero level set contour of  $\phi$ .  $\int \frac{1}{2} (|\nabla \phi(\mathbf{x})| - 1)^2 d\mathbf{x}$  is the regularization term which makes the computation accurate and stabilizes the evolution.

Secondly, fix  $f_{i,j}$ ,  $i = 1, 2, 3, 4$ ,  $j = 1, \dots, n$ , and update the level set function  $\phi_k(x)$ ,  $k = 1, 2$ . The gradient descent method is often applied to minimize the energy function with respect to the level set function  $\phi$  [19], [29]. The multi-scale fitting energy  $f_{i,j}$  are kept fixed, and the energy function is minimized by using the gradient descent method to solve the gradient flow equation:

$$\begin{aligned} \frac{\partial \phi_k}{\partial \mathbf{x}} &= -\delta_\varepsilon(\phi) F_k + v \delta_\varepsilon(\phi_k) \operatorname{div} \left( \frac{\nabla \phi_k}{|\nabla \phi_k|} \right) \\ &- \gamma_2 \delta_\varepsilon(\phi) L_k + \mu (\nabla^2 \phi_k - \operatorname{div} \left( \frac{\nabla \phi_k}{|\nabla \phi_k|} \right)) \end{aligned} \quad (3)$$

where

$$F_1 = \sum_{j=1}^4 N_j^\varepsilon(\phi_1, \phi_2) \cdot e_j$$

$$F_2 = \sum_{j=1}^4 \tilde{N}_j^\varepsilon(\phi_1, \phi_2) \cdot e_j$$

$$L_1 = (ee_2 - ee_1)$$

$$L_2 = (ee_4 - ee_3)$$

$$N_i^\varepsilon(\phi_1, \phi_2) = \lambda_i \delta_\varepsilon(\phi_1) (I - H_\varepsilon(\phi_2)), \quad i = 1, 2$$

$$N_k^\varepsilon(\phi_1, \phi_2) = \lambda_k \delta_\varepsilon(\phi_1) H_\varepsilon(\phi_2), \quad k = 3, 4$$

$$\tilde{N}_i^\varepsilon(\phi_1, \phi_2) = \lambda_i \delta_\varepsilon(\phi_2) (I - H_\varepsilon(\phi_1)), \quad i = 1, 2$$

$$\tilde{N}_k^\varepsilon(\phi_1, \phi_2) = \lambda_k \delta_\varepsilon(\phi_2) H_\varepsilon(\phi_1), \quad k = 3, 4$$

$$e_i = \sum_{j=1}^n w_j \int K_{\sigma_j}(\mathbf{y} - \mathbf{x}) |I(\mathbf{x}) - f_{i,j}(\mathbf{y})|^2 d\mathbf{x}, \quad i = 1, 2, 3, 4$$

$$ee_i = \int P(I(\mathbf{x}))_{\Omega_i} \log (P(I(\mathbf{x}))_{\Omega_i} / P(I(\mathbf{x}))_{\Omega_i \setminus C_i}) d\mathbf{x}, \quad i = 1, 2$$

$$ee_k = \int P(I(\mathbf{x}))_{\Omega_k} \log (P(I(\mathbf{x}))_{\Omega_k} / P(I(\mathbf{x}))_{\Omega_k \setminus C_2}) d\mathbf{x}, \quad k = 3, 4$$

The updating schemes can be found in Algorithm 1. When  $m = 1$ , then  $N = 2^m = 2$ , we obtain the KL-MLBF model, Which is a special case of KL-MMLBF model with one level set only[18].

In terms of numerical implementation, the calculation of the local fitting mean in the proposed MLBF model and MMLBF model requires roughly  $n$  times that in traditional local binary fitting model ( $n$  is the number of Gaussian kernel). However, despite of the increase in the computational complexity, our model converges faster in parallel implementation than LBF, because MMLBF can calculate in parallel  $N \times n$  local fitting means, and the number of iterations computation is reduced.

### III. EXPERIMENTAL RESULTS AND PERFORMANCE ANALYSIS

We apply the KL-MMLBF model on various images and compare the segmentation results with three existing approaches: LBF, LCV and LGIF. A HP desktop is used for the experiments: Intel(R) Core (TM) i5-3470 CPU, 3.20 GHz, 4 GB RAM, and Matlab 2011b on Windows 7. For all the experiments, the time step  $\Delta t$  for iteration is set to 0.1, the parameters  $\lambda_1$ ,  $\lambda_2$ ,  $\lambda_3$ ,  $\lambda_4$  and  $\nu$  are all set to 1, and the number of multi-scale kernel  $n$  is set to 3. The parameter  $\mu$  of the length constraint term varies with images.

---

#### Algorithm 1 KL-MMLBF model

---

**Input:** the parameters  $\lambda_1 = \lambda_2 = \lambda_3 = \lambda_4 = \nu = 1$ ,  $\Delta t = 1$ , the number of multi-scale kernel  $n = 3$ , the number of level set  $m = 2$ .

**Output:** the whole energy functional for segmentation  $\varepsilon(\phi)$ ;

For  $j = 1, 2, \dots, n$

For  $i = 1, 2, \dots, 2^m$

Calculate the multi-scale kernel  $k_{\sigma_j}$

Calculate the Gaussian probability distribution

$$P(I(y)|x) = \frac{1}{(2\pi)^{1/2} \sigma_j} \exp \left( -\frac{|I(y) - U_i(x)|^2}{2\sigma_j^2} \right) \quad (4)$$

For  $k=1, 2$

Fix the level set function, update  $\phi_k(x)$ , update  $f_{i,j}$ , according to Equation (2).

End for (k)

End for (i)

End for (j)

For  $j = 1, 2, \dots, n$

For  $i = 1, 2, \dots, 2^m$

For  $k=1, 2$

Fix  $f_{i,j}$ , update the level set function  $\phi_k(x)$ , according to Equation (3) by the gradient descent method.

End for (k)

End for (i)

End for (j)

---

### A. Accuracy of Contour Location

The effectiveness of the KL-MMLBF model is evaluated by applying it to both synthetic and medical images, as shown in Fig. 3. The first column in Fig. 3 illustrates the initial contours and the second to the fifth column are the segmentation results by using LBF, LGIF, LCV and our KL-MMLBF model respectively. The images shown in Fig. 3 from top to bottom are denoted as the image 1 to the image 10. The experimental results show that the segmentation of LBF model is comparatively better than the LCV model and the LGIF model, which energy function is constructed for non-uniform images, but have some issues for the image 9 and 10. Although the local-order energy is introduced to reduce the number of local optimal solutions, the LGIF model is still trapped in the local optimal solution, which leads to the unsatisfactory segmentation results. Instead the proposed model seeks the global optimum solution by introducing KL energy, namely global information. by the result that the KL-MMLBF model has better segmentation ability than the other three models.

We also apply KL-MMLBF to the natural images from the Berkeley segmentation dataset BSDS300 [30], which contains more than 300 images. More than 100 images are randomly selected from the dataset for the experiment. Representatively, here the segmentation results of 6 images are shown in Fig. 4. The columns in Fig. 4 from left to right are the original images, the manual segmentation results, the results obtained with LBF, LGIF, LCV and KL-MMLBF, respectively. It can be clearly seen that KL-MMLBF has achieved the result which is closer to that of the manual segmentation than the other three models. Table I presents the evaluation results using the metric with  $e_{mean}$  [31] in Fig. 4. It can be seen that KL-MMLBF has the lowest  $e_{mean}$  scores, indicating its superior performance over other models.

TABLE I  
EVALUATION RESULTS USING THE METRIC WITH  $e_{mean}$  [31] IN FIG. 4

Test images	LBF	LCV	LGIF	KL-MMLBF
1	2.1986	7.4150	0.1588	<b>0.1382</b>
2	1.8291	1.5925	0.9890	<b>0.6015</b>
3	15.2778	2.5773	12.8043	<b>0.2796</b>
4	10.778	3.7735	12.3804	<b>2.2796</b>
5	7.854	5.3236	4.4741	<b>3.8701</b>
6	8.7278	2.3273	2.0883	<b>1.8129</b>

### B. Speed of Evolution Convergence

The KL-MMLBF's efficiency can be reflected by the iteration times required for obtaining the final contour and the total CPU time taken to complete the segmentation. The iteration times and the CPU time required for the segmentation as in Fig. 3 and Fig. 4 are shown in Table II and Table III. Table II tells that KL-MMLBF requires fewer iteration times than the other three models in general. From Table III, it is obvious that only the iteration times of LCV model for segmenting the image 4 is less than that of KL-MMLBF. This is because the LCV model falls into a local optimum, which needs fewer iteration times. But the segmentation result of LCV is worse than that of KL-MMLBF as shown in Fig. 4.

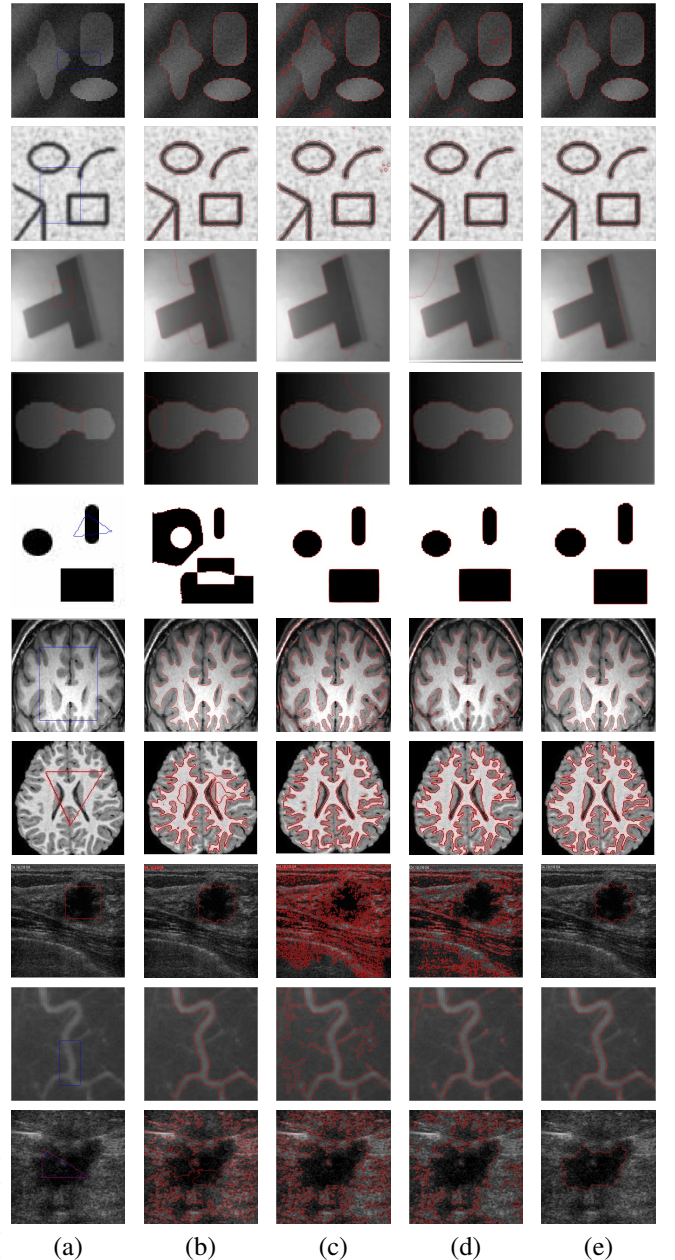


Fig. 3. Comparison of the segmentation results with synthetic and medical images. (a) Original images, (b) LBF, (c) LGIF, (d) LCV, (e) KL-MMLBF

Worth to note that, the CPU time spent for LGIF to obtain the final segmentation results is less than that for KL-MMLBF in four images. However the segmentation results of these images are rather poor, as shown in Fig. 4, and the reason is the same as in analysis of Table II. In contrast, the segmentation results of KL-MMLBF are more accurate than the other three models, and it has been proved objectively in the section III.A.

### C. Robustness Against Initial Position

In order to validate the KL-MMLBF's robustness to the initial position of the level set, we compared it with LBF, LGIF and Order-LBF [32]. Fig. 5 shows the experimental results of medical images which are typical with intensity inhomogeneity. Note that the characteristics of some vessel



Fig. 4. Comparison of the segmentation results with natural images

TABLE II  
COMPARISON OF SPEED FOR THE EXPERIMENT SHOWN IN FIG. 3

Test images (image size)	LBF		LGIF		LCV		KL-MMLBF	
	CPU time(s)	Iterations	CPU time(s)	Iterations	CPU time(s)	Iterations	CPU time(s)	Iterations
1(79*75)	4.5934	250	9.1589	300	3.6374	200	<b>2.1246</b>	<b>110</b>
2(95*72)	0.80496	40	3.2876	100	2.8183	150	<b>0.66016</b>	<b>30</b>
3(111*110)	1.924	95	5.7829	147	2.963	150	<b>1.3253</b>	<b>60</b>
4(103*131)	6.274	300	5.1286	147	3.8407	200	<b>2.1782</b>	<b>100</b>
5(252*185)	2.9208	90	7.3743	100	3.5102	130	<b>2.3652</b>	<b>70</b>
6(119*78)	3.4654	185	6.7317	190	<b>3.3102</b>	190	3.5017	<b>180</b>
7(180*170)	4.0258	180	9.7792	190	<b>3.773</b>	190	4.0474	<b>180</b>
8(549*357)	69.7826	350	87.7608	350	78.6312	350	<b>67.3824</b>	<b>300</b>
9(252*185)	2.9208	94	7.3743	105	3.5202	100	<b>2.3652</b>	<b>80</b>
10(252*185)	3.4654	100	6.7317	110	3.5109	90	<b>3.0217</b>	<b>85</b>

TABLE III  
COMPARISON OF SPEED FOR THE EXPERIMENT SHOWN IN FIG. 4

Test images (image size)	LBF		LGIF		LCV		KL-MMLBF	
	CPU time(s)	Iterations	CPU time(s)	Iterations	CPU time(s)	Iterations	CPU time(s)	Iterations
1(481*321)	28.0367	230	<b>7.4294</b>	200	21.8822	200	18.4019	<b>150</b>
2(481*321)	28.2309	220	<b>10.0456</b>	220	21.782	<b>190</b>	25.3336	200
3(481*321)	61.5956	500	<b>13.6884</b>	300	21.8537	180	18.9407	<b>150</b>
4(481*321)	30.0458	500	34.8194	600	73.4609	900	<b>29.9546</b>	<b>290</b>
5(481*321)	29.2190	500	<b>18.3457</b>	300	29.1878	400	24.4507	<b>100</b>
6(481*321)	30.2 66	260	22.9769	220	22.4559	220	<b>19.8737</b>	<b>200</b>

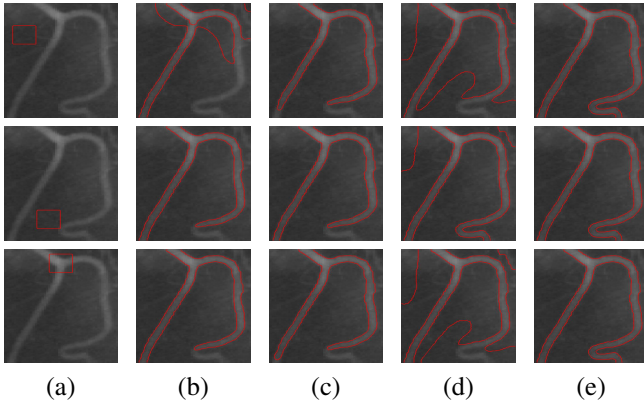


Fig. 5. Segmentation results with different initial locations: (a) initial contour, (b) LBF, (c) LGIF, (d) Order-LBF, (e) KL-MMLBF

regions are quite weak, which renders it a nontrivial task to segment the vessels in the images. Fig. 5(a) shows various initial contours for the vessels image, while the corresponding segmentation results of LBF, LGIF, Order-LBF and KL-MMLBF are shown from Fig. 5(b) to Fig. 5(e), respectively. From the results shown in Fig. 5(b) and Fig. 5(c), we can see that, though LBF and LGIF are able to handle the intensity inhomogeneity to certain extent, they are sensitive to the initial position of the level set. Especially, the continuously shrinking level set leads to the worst results shown in the row 2 and the column (b), failing to detect any contour. In other words, if a better initial contour is chosen, LBF and LGIF can produce satisfactory segmentation results; otherwise, these two models will only achieve a local solution which doesn't satisfy the global optimization. The Order-LBF model in the Fig. 5(d) can obtain almost the same segmentation results for various initial contours, demonstrating its global property. However, it can't achieve the optimal segmentation results. The results in the Fig. 5(e) show that KL-MMLBF is more capable to cope with the intensity inhomogeneity. The results prove that KL-MMLBF is robust for initial contour and effective to deal with the problems caused by intensity inhomogeneity.

#### D. Robustness Against Noise

To verify the robustness of KL-MMLBF to noise, firstly the experiments are performed on images contaminated by various degrees of Gaussian noise, whose standard deviations are 0, 15, 20, 25. Segmentation results are shown in Fig. 6, in which the red curve indicates the position of initialized zero level set, and the green curve is the final segmentation results. In Fig. 6, row 1-2, row 3-4 and row 5-6 show the segmentation results of LBF model, Order-LBF model and KL-MMLBF model, respectively. It can be seen that, compared with LBF model, Order-LBF model has stronger robustness to noise, but in some cases, still cannot segment correctly, while KL-MMLBF model can effectively segment target contours in various situations. Because the KL energy in the proposed model enhances the differences between regions, the noise can be processed accurately and better segmentation results can be obtained. The energy functions are constructed based on local information in other models, therefore, the accuracy

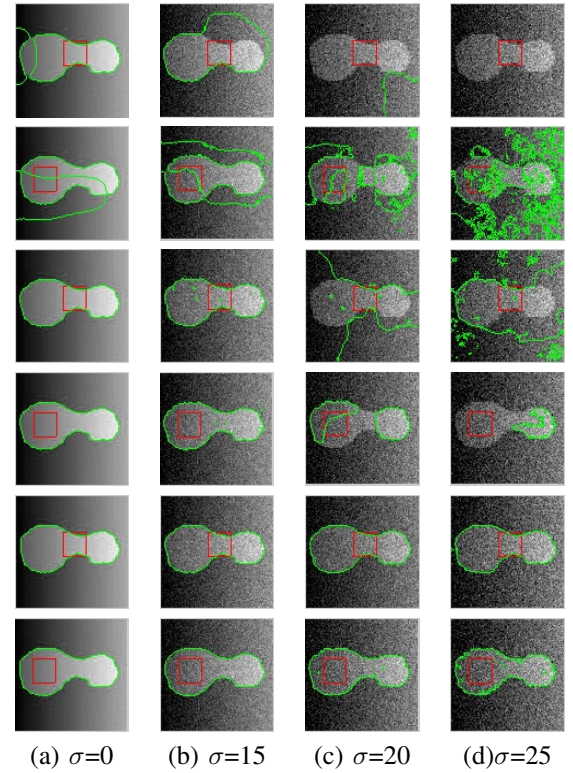


Fig. 6. Comparison of image segmentation results with various degrees of Gaussian noises

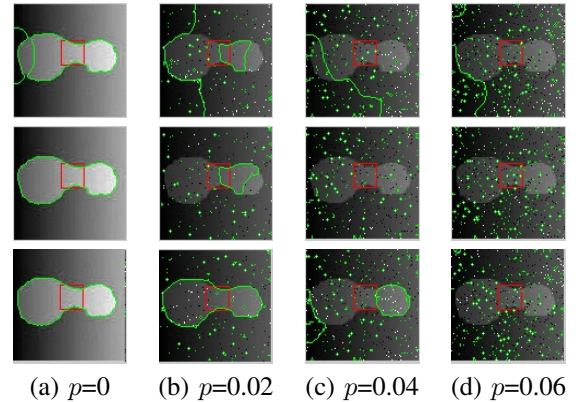


Fig. 7. Comparison of segmentation results of images with different levels of salt and pepper noise (Where P is the parameter of Salt Pepper noise in Matlab)

of segmentation will be seriously affected by the noise, the segmentation result becomes worse as the noise increases. Compared with other models, KL-MMLBF model can obtain better segmentation results, and has good robustness to noise. Moreover, it can be observed that, in the experiment of Gauss noise, the number of iterations to segment the target contours are increased with the increase of the degree of noise pollution.

Then the experiments are performed on images contaminated by different level Salt and Pepper noise. In the experiment, the model parameters are same as that for Gaussian noise (in Fig. 6). Comparative experimental results are shown in Fig. 7, in which the red curve indicates the position of initialized zero level set, and the green curve indicates the final segmentation results. From the top to bottom rows show

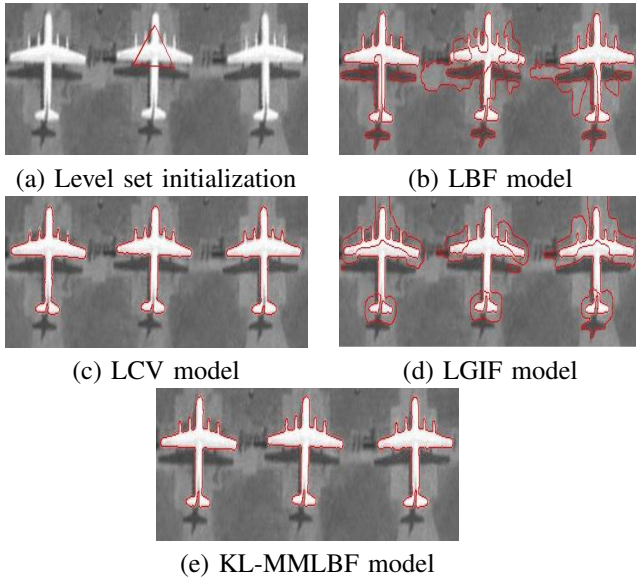


Fig. 8. Segmentation results of multi-phase multi-scale image segmentation model ( $\phi_1$  and  $\phi_2$  have same initialization)

segmentation results of LBF model, Order-LBF model, kl-MMLBF model, respectively. According to the segmentation results we can conclude that, compared with other models, KL-MMLBF model has better robustness to Salt and pepper noise. Despite of this, all models have poor robustness to salt and pepper noise. The main reason is that the mean fitting kernel function of each model for the experiments is Gaussian function, which has inherent capability of de-noising for the Gaussian noise. Meanwhile, the weighted average with Gaussian kernel is performed in calculating the local energy fitting item, so it is possible to further reduce the impact of Gaussian noise. However for salt and pepper noise, it is known that the rank-order based filter, especially the median filter has good inhibitory effect on the salt and pepper noise, while the Gaussian low-pass filter is not effective on the salt and pepper noise. Therefore, the poor robustness of the model on salt and pepper noise robustness is mainly caused by using the Gaussian kernel function which is not effective on salt and pepper noise.

#### E. Multi-region Image Segmentation

The Fig.8 and Fig.9 are multi-region images. In Fig.8, the segmentation results of the LCV model are better than those of the LBF model and the LGIF model, and are also comparable with the results of the KL-MMLBF model. The LCV model, to some extent, is a CV model. The results shown in Fig. 8(b) also demonstrate that the LBF model is not a good model to segment the almost piece-wise image. The LGIF model which is a combination of the CV model and to some degree the LBF model is not appropriate too. It is obvious that the KL-MMLBF model outperforms the LBF model, LCV model and the LGIF model in this case.

Overall, we can conclude from the results in Fig.8 (where  $\phi_1$  and  $\phi_2$  have same initialization) and Fig.9 (where  $\phi_1$  and  $\phi_2$  have different initialization) that, LBF, LCV and LGIF, in some cases, can offer better segmentation results which are

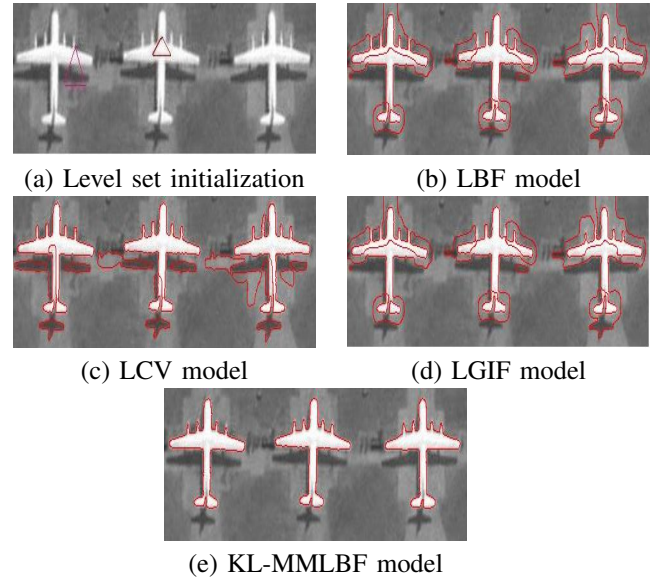


Fig. 9. Segmentation results of multi-phase multi-scale image segmentation model ( $\phi_1$  and  $\phi_2$  have different initialization)

comparable with that of the KL-MMLBF model. However, the results also show that these comparing models are unstable for the initial position. It has been demonstrated that the KL-MMLBF model is more stable and has the fine properties of both the global information based model and the local information based model.

#### IV. CONCLUSION

In this paper, we have proposed a level set method for image segmentation based on multi-region multi-scale local binary fitting model(MMLBF) and Kullback-Leibler (KL) divergence. The construction of MMLBF is based on the LBF model, in which the Gaussian kernels with different scale parameters and multi-phase level set framework are introduced to deal with the segmentation of inhomogeneous images. We have introduced a new energy term represented by the KL divergence into MMLBF to estimate the between-cluster distance energy. The experiments on synthetic images, medical images and natural images from the Berkeley BSDS300 dataset have demonstrated that KL-MMLBF can achieve more accurate segmentation results than existing approaches such as LBF, LGIF, LCV and Order-LBF. In terms of robustness, our experiments have proved that KL-MMLBF are more robust to noise and initial contour than other models. However, KL-MMLBF faces difficulty on the increase of the computational complexity. In our future work, We will analyze the approach to find ways to reduce its complexity.

#### ACKNOWLEDGMENT

This research was supported by the National Natural Science Foundation of China (Grant No. 61402133).

#### REFERENCES

- [1] T. Liu, Z. Yuan, J. Sun, J. Wang, N. Zheng, X. Tang, and H.-Y. Shum, "Learning to detect a salient object," *Pattern Analysis and Machine Intelligence, IEEE Transactions on*, vol. 33, no. 2, pp. 353–367, 2011.

- [2] D. Cheng, X. Liu, Y. Jin, and J. Liu, "Multi-level image fuzzy enhancement based on neighborhood," *Journal of Harbin Institute of Technology*, vol. 43, no. 7, pp. 85–89, 2011.
- [3] Y. H. Tsai, M. H. Yang, and M. J. Black, "Video segmentation via object flow," in *IEEE Conference on Computer Vision and Pattern Recognition*, 2016, pp. 3899–3908.
- [4] A. Parsi, A. G. Sorkhi, and M. Zahedi, "Improving the unsupervised lbg clustering algorithm performance in image segmentation using principal component analysis," *Signal Image Video Processing*, vol. 10, no. 2, pp. 301–309, 2016.
- [5] D. Cheng, J. Huang, Z. Yu, X. Tang, and J. Yang, "Medical image enhancement based on fuzzy techniques," *Journal of Harbin Institute of Technology*, vol. 39, no. 3, pp. 435–437, 2007.
- [6] A. W. M. and D. Terzopoulos, "Snakes: Active contour models," *Int. J. Comput. Vis.*, vol. 1, no. 4, pp. 321–331, 1988.
- [7] D. Reska, C. Boldak, and M. Kretowski, "Towards multi-stage texture-based active contour image segmentation," *Signal Image Video Processing*, pp. 1–8, 2016.
- [8] F. C. V. Casselles and F. Dibos, "A geometric model for active contours in image processing," *Numer. Math.*, vol. 66, no. 1, pp. 1–31, 1993.
- [9] E. J. Candès, X. Li, Y. Ma, and J. Wright, "Robust principal component analysis?" *Journal of the ACM (JACM)*, vol. 58, no. 3, p. 11, 2011.
- [10] L. A. Vese and T. F. Chan, "A multiphase level set framework for image segmentation using the mumford and shah model," *International journal of computer vision*, vol. 50, no. 3, pp. 271–293, 2002.
- [11] L. S. Cigaroudy and N. Aghazadeh, "A multiphase segmentation method based on binary segmentation method for gaussian noisy image," *Signal Image Video Processing*, pp. 1–7, 2016.
- [12] C. Li, C.-Y. Kao, J. C. Gore, and Z. Ding, "Implicit active contours driven by local binary fitting energy," in *Computer Vision and Pattern Recognition, 2007. CVPR'07. IEEE Conference on*. IEEE, 2007, pp. 1–7.
- [13] D. Cheng, X. Liu, J. Liu, and X. Tang, "Image segmentation using neighborhood inspiring pulse coupled neural network," *Journal of Huazhong University of Science and Technology(Nature Science Edition)*, vol. 37, no. 5, pp. 33–37, 2009.
- [14] A. Ahmadvand and P. Kabiri, "Multispectral mri image segmentation using markov random field model," *Signal Image Video Processing*, vol. 10, no. 2, pp. 251–258, 2016.
- [15] H. Bakir, M. Charfi, and J. Zrida, "Automatic active contour segmentation approach via vector field convolution," *Signal Image Video Processing*, vol. 10, no. 1, pp. 1–10, 2016.
- [16] X.-F. Wang, D.-S. Huang, and H. Xu, "An efficient local chan-vese model for image segmentation," *Pattern Recognition*, vol. 43, no. 3, pp. 603–618, 2010.
- [17] L. Wang, C. Li, Q. Sun, D. Xia, and C.-Y. Kao, "Active contours driven by local and global intensity fitting energy with application to brain mr image segmentation," *Computerized Medical Imaging and Graphics*, vol. 33, no. 7, pp. 520–531, 2009.
- [18] L. Liu, D. Cheng, F. Tian, D. Shi, and R. Wu, "Active contour driven by multi-scale local binary fitting and kullback-leibler divergence for image segmentation," *Multimedia Tools Applications*, vol. 76, no. 7, pp. 1–20, 2017.
- [19] S. Kullback and R. A. Leibler, "On information and sufficiency," *The annals of mathematical statistics*, pp. 79–86, 1951.
- [20] T. Brox and J. Weickert, "Level set based image segmentation with multiple regions," in *Pattern recognition*. Springer, 2004, pp. 415–423.
- [21] N. Paragios and R. Deriche, "Coupled geodesic active regions for image segmentation: A level set approach," in *Computer Vision/ECCV 2000*. Springer, 2000, pp. 224–240.
- [22] A. Vazquez-Reina, E. Miller, and H. Pfister, "Multiphase geometric couplings for the segmentation of neural processes," in *Computer Vision and Pattern Recognition, 2009. CVPR 2009. IEEE Conference on*. IEEE, 2009, pp. 2020–2027.
- [23] Z. Shahvaran, K. Kazemi, and M. S. Helfroush, "Simultaneous vector-valued image segmentation and intensity nonuniformity correction using variational level set combined with markov random field modeling," *Signal Image Video Processing*, vol. 10, no. 5, pp. 887–893, 2016.
- [24] A. Yezzi, A. Tsai, and A. Willsky, "A fully global approach to image segmentation via coupled curve evolution equations," *Journal of Visual Communication and Image Representation*, vol. 13, no. 1, pp. 195–216, 2002.
- [25] H.-K. Zhao, T. Chan, B. Merriman, and S. Osher, "A variational level set approach to multiphase motion," *Journal of computational physics*, vol. 127, no. 1, pp. 179–195, 1996.
- [26] C. Samson, L. Blanc-Féraud, G. Aubert, and J. Zerubia, "A level set model for image classification," *International Journal of Computer Vision*, vol. 40, no. 3, pp. 187–197, 2000.
- [27] A. Yezzi Jr, A. Tsai, and A. Willsky, "A statistical approach to snakes for bimodal and trimodal imagery," in *Computer Vision, 1999. The Proceedings of the Seventh IEEE International Conference on*, vol. 2. IEEE, 1999, pp. 898–903.
- [28] M. E. Leventon, W. E. L. Grimson, and O. Faugeras, "Statistical shape influence in geodesic active contours," in *Computer Vision and Pattern Recognition, 2000. Proceedings. IEEE Conference on*, vol. 1. IEEE, 2000, pp. 316–323.
- [29] S. Balla-Arabé, X. Gao, and B. Wang, "A fast and robust level set method for image segmentation using fuzzy clustering and lattice boltzmann method," *Cybernetics, IEEE Transactions on*, vol. 43, no. 3, pp. 910–920, 2013.
- [30] D. Martin, C. Fowlkes, D. Tal, and J. Malik, "A database of human segmented natural images and its application to evaluating segmentation algorithms and measuring ecological statistics," in *Computer Vision, 2001. ICCV 2001. Proceedings. Eighth IEEE International Conference on*, vol. 2. IEEE, 2001, pp. 416–423.
- [31] C. Li, C. Xu, C. Gui, and M. D. Fox, "Distance regularized level set evolution and its application to image segmentation," *Image Processing, IEEE Transactions on*, vol. 19, no. 12, pp. 3243–3254, 2010.
- [32] L. Wang, Z. Yu, and C. Pan, "Medical image segmentation based on novel local order energy," in *Computer Vision—ACCV 2010*. Springer, 2011, pp. 148–159.